

SMAFormer: Synergistic Multi-Attention Transformer for Medical Image Segmentation

Fuchen Zheng¹², Xuhang Chen¹²³, Weihuang Liu¹, Haolun Li¹, Yingtie Lei¹⁴, Jiahui He²⁵,
Chi-Man Pun^{1*}, and Shoujun Zhou^{2*}

¹University of Macau

²Shenzhen Institutes of Advanced Technology, Chinese Academy of Sciences

³Huizhou University

⁴The Ohio State University

⁵University of Nottingham Ningbo China

Abstract—In medical image segmentation, specialized computer vision techniques, notably transformers grounded in attention mechanisms and residual networks employing skip connections, have been instrumental in advancing performance. Nonetheless, previous models often falter when segmenting small, irregularly shaped tumors. To this end, we introduce SMAFormer, an efficient, Transformer-based architecture that fuses multiple attention mechanisms for enhanced segmentation of small tumors and organs. SMAFormer can capture both local and global features for medical image segmentation. The architecture comprises two pivotal components. First, a Synergistic Multi-Attention (SMA) Transformer block is proposed, which has the benefits of Pixel Attention, Channel Attention, and Spatial Attention for feature enrichment. Second, addressing the challenge of information loss incurred during attention mechanism transitions and feature fusion, we design a Feature Fusion Modulator. This module bolsters the integration between the channel and spatial attention by mitigating reshaping-induced information attrition. To evaluate our method, we conduct extensive experiments on various medical image segmentation tasks, including multi-organ, liver tumor, and bladder tumor segmentation, achieving state-of-the-art results. Code and models are available at: <https://github.com/lzeeorno/SMAFormer>.

Index Terms—Transformer, Tumor Segmentation, Medical Image Segmentation, Feature Fusion, Attention Mechanism

I. INTRODUCTION

Medical image segmentation tasks based on artificial intelligence play a crucial role in clinical adjunctive therapy. This is because the failure to diagnose tumors at an early stage often leads to the advancement of cancer [1], rendering it incurable. Nevertheless, the challenge lies in the feature loss in various tiny tumors or organs after deep convolutions, making the task of medical image segmentation based on artificial intelligence highly demanding.

Recent state-of-the-art methods [2]–[8] are primarily based on Convolutional Neural Networks (CNNs), which achieve impressive results but exhibit limitations in capturing features of small objects. To address this issue, several recent studies [9], [10] have employed multi-attention mechanisms in

feature maps. However, the results are still suboptimal, and the various attention mechanisms do not integrate well.

In this paper, we aim to leverage the capability of multi-attention fusion in feature maps at multiple scales to capture in-depth image details. Accordingly, we present SMAFormer, a Transformer-based architectural design that is both effective and computationally efficient for medical image segmentation tasks. Drawing inspiration from the ResUNet framework [11], our SMAFormer model unites Transformer blocks with a U-shaped residual structure to enhance feature learning across multiple resolutions.

First, we propose the Synergistic Multi-Attention (SMA) Transformer block, which conducts pixel-wise self-attention and integrates features from channel-wise and spatial attention within its feed-forward pathway. Recognizing the importance of capturing extensive global dependencies in hierarchical feature representations, we draw inspiration from recent literature [12], [13] to design a learnable multi-scale segmentation modulator. This modulator, embedded as a multi-scale spatial bias, is pivotal for preserving salient features across varying scales in both encoding and decoding stages. Specifically, additional self-adaptive bias is incorporated within each SMA block to facilitate optimal fusion when multiple attention types are merged. Consequently, our straightforward residual U-shaped Transformer design, without elaborate multi-scale architectures [14], [15] or sophisticated loss strategies [16], [17], attains leading performance in diverse medical image segmentation challenges. Notably, in tumor segmentation, SMAFormer surpasses the prior state-of-the-art model, Swin UNETR [7], achieving improvements of 1.63% and 2.18% in dice score coefficient on the LiTS2017 and ISICDM2019 datasets, respectively.

The main contributions of this paper are as follows:

- 1) We propose **SMAFormer**, a residual U-shaped Transformer model designed for diverse medical image segmentation tasks. SMAFormer integrates the attention mechanism, U-shaped architecture, and residual connections, resulting in a model that is both efficient and effective.

* Corresponding Authors.

- 2) We design an embeddable and learnable segmentation modulator to fuse multi-scale features. This module significantly enhances the cooperative effect among diverse attention mechanisms.
- 3) Extensive experiments demonstrate that the proposed SMAFormer achieves new state-of-the-art results on various medical image segmentation datasets.

II. RELATED WORK

A. Medical Image Segmentation

Medical image segmentation constitutes the division of structures or tissues within medical images into distinct regions or objects. Among the various methodologies, the U-Net architecture [18] has attained prominence due to its sophisticated design and capacity for precise detail extraction while preserving contextual information. This has prompted a proliferation of innovative derivatives, with ResUNet [11] emerging as a prominent adaptation, integrating the strengths of U-Net [18] and ResNet [19].

ResNet's introduction of residual connections [20] revolutionized deep learning by mitigating the vanishing gradient problem, facilitating the training of deeper networks through uninterrupted information flow across layers [21]. This residual learning framework significantly enhances image segmentation capabilities.

The synergy of residual connections and skip connections in ResUNet constructs a highly efficient segmentation model, where the former ensures unimpeded information transfer and the latter facilitates comprehensive feature integration. This combination propels ResUNet to excel in diverse image segmentation challenges. While U-Net effectively recovers spatial information through upsampling and expands receptive fields via downsampling, it initially lacked inter-layer communication. To overcome this, UNet++ [22] innovated by introducing intermediary nodes with feature concatenation-based long connections, thereby enhancing intra-layer information sharing. Reflecting these advancements, SMAFormer also embraces fundamental yet potent designs, including skip connections and residual connections, to optimize segmentation performance.

B. Vision Transformer

Transformer-based network structures, unlike the design of CNNs, excel at capturing long-range dependencies in images through global self-attention mechanisms. The pioneering work of Vision Transformer (ViT) [23] has demonstrated superior performance compared to state-of-the-art CNNs in image classification. Moreover, transformers have gained significant traction in medical imaging applications due to their robust feature extraction capabilities, as exemplified by the Swin Transformer [24]. Researchers have also explored the fusion of ResNet and transformer models, resulting in powerful architectures such as ResT [25], [26]. In the context of U-Net, incorporating attention units [27] enables the network to focus on segmenting multiple objects, leading to the integration of attention mechanisms into U-Net architectures and the

creation of U-shaped transformers. Chen *et al.* [5] propose TransUNet to explore the potential of transformers in medical image segmentation. The overall architecture of TransUNet employs a convolutional network as a feature extractor and a transformer to encode global context. However, a common issue with TransUNet and similar works [4], [28] is that the advantages provided by the transformer component are not fully exploited, and although various attention mechanisms have been combined, their integration remains suboptimal. To address this, we have designed a general residual U-shaped Transformer-based structure, which has been proven to be efficient and effective for attention fusion, aiming to enhance performance in medical image segmentation.

III. METHOD

This section details the architecture and functionality of SMAFormer, a novel Transformer-based network designed for medical image segmentation. We begin by outlining the overall pipeline of the network, followed by a comprehensive description of the SMA Transformer block, the fundamental building block of SMAFormer. Finally, we elaborate on the role of the multi-scale segmentation modulator in facilitating synergistic multi-attention and enhancing the network's ability to capture fine-grained details.

A. Overall Pipeline

SMAFormer, as depicted in Figure 1, adopts a hierarchical U-shaped architecture reminiscent of ResU-Net [29], [30], incorporating skip-connections and residual connections between the encoder and decoder for efficient information propagation.

Given a 3D medical image $I \in \mathbb{R}^{3 \times H \times W}$, SMAFormer first extracts low-level features through an initial projection layer comprising a 3×3 convolution followed by a ReLU activation. The extracted features are then passed through a four-stage encoder, mirroring the U-Net structure. Each encoder stage consists of a stack of SMA Transformer blocks (detailed in Section III-B) for capturing multi-scale features, followed by a down-sampling layer.

The down-sampling layer performs two crucial operations. First, it records positional information within the embedded modulator (discussed in Section III-C). Second, it utilizes a residual convolution block which consist by three 3×3 convolutions with a stride of 2 to reduce the spatial dimensions of the feature maps while increasing the channel count. This down-sampling process is enriched by residual connections, enabling the preservation of long-range dependencies. Specifically, given an input feature map $X_i \in \mathbb{R}^{C \times H \times W}$, the output of the i -th encoder stage is $X_{\text{conv}} + X_{\text{residual}} \in \mathbb{R}^{2^i C \times \frac{H}{2^i} \times \frac{W}{2^i}}$, where X_{conv} denotes the convolved features and X_{residual} represents the features from the residual connection.

Mirroring the encoder, the decoder comprises four symmetrical stages. Each stage begins with a 2×2 transposed convolution to upsample the feature maps, effectively halving the channel count and doubling the spatial dimensions. Subsequently, the upsampled features are concatenated with

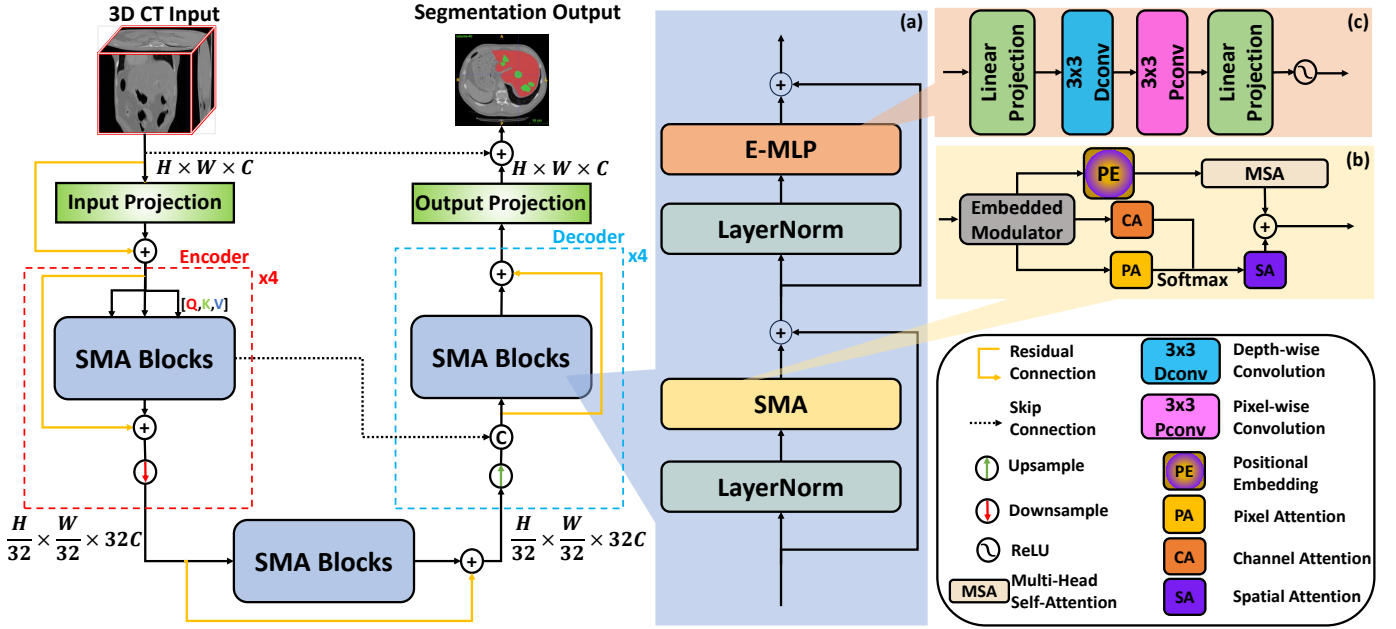


Fig. 1. This figure provides an overview of the SMAFormer architecture. The figure details (a) the SMA Transformer block, (b) the SMA Part within the SMA Transformer block, and (c) the E-MLP Part within the SMA Transformer block.

the corresponding encoder features via skip connections, facilitating the fusion of high-level semantic information with low-level spatial details. Finally, an output convolution layer processes the concatenated features to generate the segmentation prediction.

B. SMA Transformer Block

Directly applying conventional Transformers to medical image segmentation presents two significant challenges: (1) **Difficulty in Assigning Attention to Relevant Regions:** Transformers, especially when not fine-tuned for medical images, often struggle to focus attention on medically relevant regions, hindering their performance in multi-organ or multi-tumor segmentation tasks. (2) **Limited Capture of Local Context:** Local context plays a crucial role in accurately segmenting small structures like organs or tumors. Traditional Transformers, with their global receptive fields, often fail to adequately capture this local information.

To address these challenges, we introduce the Synergistic Multi-Attention (SMA) Transformer block, illustrated in Figure 1. This block leverages the combined strengths of three distinct attention mechanisms and multi-head self-attention to achieve robust and accurate segmentation.

1) *Synergistic Multi-Attention (SMA):* Unlike approaches that restrict self-attention within local windows [30], SMA employs a combination of channel attention, spatial attention, and pixel attention in conjunction with multi-head self-attention. This synergistic approach enables the model to effectively capture multi-scale features and handle potential deformations within the medical images as depicted in Figure 1 (b). Given a feature map $X \in \mathbb{R}^{C \times H \times W}$, SMA first divides it into patches and flattens the channels. The flattened features are

then processed by the three attention mechanisms (channel attention, pixel attention, and spatial attention) in parallel. The outputs from the pixel and channel attention branches are combined through matrix multiplication and further processed by the spatial attention branch. Finally, the outputs from all three branches are fused to generate the final attention map.

2) *Enhanced Multi-Layer Perceptron (E-MLP):* Recognizing the limitations of standard Feed-Forward Networks (FFNs) in capturing local context [31], [32], we enhance the E-MLP within our Transformer block by incorporating depth-wise and pixel-wise convolutions [33]–[35]. As depicted in Figure 1 (c), the E-MLP first projects the input tokens to a higher dimensional space using a linear layer. The projected tokens are then reshaped into 2D feature maps and processed by a 3×3 pixel-wise convolution followed by a 3×3 depth-wise convolution, effectively capturing local contextual information. The resulting features are then reshaped back into tokens and projected back to the original channel dimension using another linear layer. Finally, a GELU activation function [36] is applied to introduce non-linearity.

Mathematically, the computation within an SMA Transformer block can be expressed as:

$$\begin{aligned} X'_{i+1} &= SMA(LN(X_i)) + X_i, \\ X_{i+1} &= E - MLP(LN(X'_{i+1})) + X'_{i+1}, \end{aligned} \quad (1)$$

where X_i represents the input features to the i -th block, X'_{i+1} and X_{i+1} are the outputs of the SMA and E-MLP modules respectively, and LN denotes layer normalization.

The synergistic interplay between SMA and E-MLP within each Transformer block enables SMAFormer to effectively capture both global and local contextual information, leading to improved segmentation performance.

C. Multi-Scale Segmentation Modulator

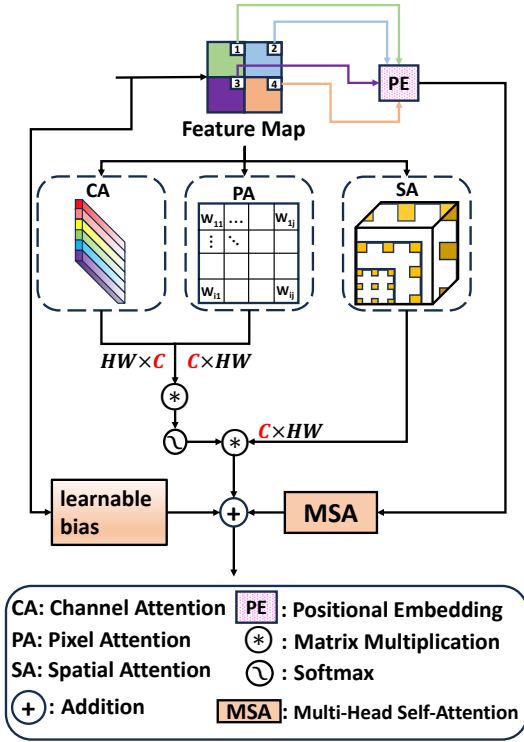


Fig. 2. This figure presents a schematic diagram of the proposed modulator.

To further enhance SMAFormer’s ability to capture fine-grained details and facilitate synergistic multi-attention, we introduce the multi-scale segmentation modulator as shown in Figure 2.

Positioned at each scale of the network, the modulator serves three primary functions:

- 1) **Positional Encoding:** The modulator embeds positional information into the feature maps, compensating for the lack of inherent positional awareness in the Transformer architecture. This is achieved through a projection convolution layer that maps the multi-scale SMA outputs from the shape $[B, H, W, C]$ to the MSA output with shape $[B, H \times W, C]$.
- 2) **Trainable Bias:** The modulator incorporates a trainable bias term, which is added to the output of the multi-head self-attention mechanism. This bias term, updated during training, helps fine-tune the attention maps and improves the model’s ability to focus on relevant regions.
- 3) **Facilitating Multi-Attention Computations:** The modulator assists in performing the necessary transpositions and matrix multiplications required for the three different attention mechanisms within the SMA block. This ensures efficient computation and seamless integration of the multi-attention module within the overall architecture.

D. Objective Function

We train SMAFormer using the BCE Dice loss \mathcal{L}_{BD} [37], a widely adopted loss function for segmentation tasks that combines the benefits of Binary Cross-Entropy (BCE) loss \mathcal{L}_{BCE} and Dice loss \mathcal{L}_D :

$$\begin{aligned} \mathcal{L}_{BD} &= \mathcal{L}_D + \mathcal{L}_{BCE}(y, p) \\ &= \frac{1}{N} \sum_{i=1}^N \left(1 - \frac{2 \sum_j y_{i,j} p_{i,j}}{\sum_j y_{i,j} + \sum_j p_{i,j}} \right) \\ &\quad - (y \log(p) + (1 - y) \log(1 - p)), \end{aligned} \quad (2)$$

where y represents the ground truth segmentation mask, p denotes the predicted segmentation mask, and N is the number of pixels in the image. The BCE loss penalizes discrepancies between the predicted and true label distributions, while the Dice loss encourages overlap between the predicted and true segmentation regions. This combined loss function encourages both accurate pixel-wise classification and strong boundary delineation.

IV. EXPERIMENTS

This section details the experimental setup and presents the results obtained. We first describe the datasets used and the evaluation metrics employed. Next, we compare the performance of SMAFormer against several state-of-the-art methods on medical image segmentation tasks. Finally, we conduct ablation studies to analyze the contribution of each component within our proposed SMAFormer architecture.

A. Datasets and Implementation Details

To ensure a comprehensive evaluation and fair comparison with existing methods, we conducted experiments on three publicly available medical image segmentation datasets:

- 1) **LiTS2017** [39]: This dataset focuses on liver tumor segmentation and comprises 131 contrast-enhanced 3D abdominal CT scans.
- 2) **ISICDM2019** [40]: This dataset centers on bladder tumor segmentation and includes 2200 bladder cancer images.
- 3) **Synapse** [41]: This dataset targets multi-organ segmentation and consists of 40 3D abdominal CT scans with multiple organs.

For all experiments, we followed the training/validation/test splits provided by nnformer [6] to ensure consistency and fair comparison with other methods. This resulted in a split of 80%, 15%, and 5% for training, validation, and testing, respectively. All input images were resized to a resolution of 512×512 pixels.

We implemented SMAFormer using the PyTorch framework and trained the model on a single NVIDIA GeForce RTX 4090 GPU. We employed the Stochastic Gradient Descent (SGD) optimizer [42] with a momentum of 0.98 and weight decay of $1e^{-6}$. The learning rate was initially set to $1e^{-2}$ and decreased using a cosine decay strategy to a minimum of $6e^{-6}$. Data augmentation during training included random horizontal flipping and rotation.

TABLE I
COMPARISON WITH STATE-OF-THE-ART MODELS ON THE ISIDM2019 AND LITS2017 DATASETS. THE BEST RESULTS ARE BOLDED WHILE THE SECOND BEST ARE UNDERLINED.

| Method | ISIDM2019 | | | | LITS2017 | | | |
|------------------------|--------------|--------------|--------------|--------------|--------------|--------------|--------------|--------------|
| | Average | | Bladder | Tumor | Average | | Bladder | Tumor |
| | DSC(%) ↑ | mIoU(%) ↑ | DSC(%) ↑ | DSC(%) ↑ | DSC(%) ↑ | mIoU(%) ↑ | DSC(%) ↑ | DSC(%) ↑ |
| ViT [23]+CUP [5] | 88.60 | 84.40 | 91.88 | 85.32 | 80.33 | 77.25 | 83.97 | 76.69 |
| R50-ViT [23]+CUP [5] | 88.77 | 85.62 | 92.05 | 85.49 | 82.62 | 79.68 | 85.83 | 79.41 |
| ResUNet++ [29] | 87.11 | 83.78 | 89.90 | 84.32 | 75.73 | 74.19 | 79.12 | 72.34 |
| ResT-V2-B [26] | 89.26 | 82.13 | 93.01 | 85.50 | 78.53 | 75.24 | 81.22 | 75.83 |
| TransUNet [5] | <u>94.56</u> | <u>93.60</u> | <u>97.74</u> | <u>91.38</u> | <u>93.28</u> | <u>90.81</u> | <u>95.54</u> | <u>91.03</u> |
| SwinUNet [3] | 91.95 | 89.77 | 94.73 | 89.17 | 89.68 | 86.62 | 93.31 | 86.04 |
| Swin UNETR [7] | 92.60 | 90.61 | 95.08 | 90.12 | 91.95 | 90.02 | 94.73 | 89.17 |
| UNETR [38] | 91.55 | 88.34 | 94.83 | 88.26 | 89.38 | 87.46 | 92.89 | 85.86 |
| nnFormer [6] | 93.54 | 89.11 | 96.97 | 90.41 | 91.74 | 89.95 | 94.57 | 88.91 |
| SMAFormer(Ours) | 96.07 | 94.67 | 98.57 | 93.56 | 94.11 | 91.94 | 95.88 | 92.34 |

We use a pre-trained model from [43]. The results of experiment are the mean of Five-Fold Cross-Validation. Part of results from [6] and [44].

B. Evaluation Metrics

We evaluated the segmentation performance using two widely adopted metrics:

Dice Coefficient Score (DSC) [46]: DSC measures the overlap between the predicted segmentation and the ground truth. It ranges from 0 to 1, with higher values indicating better segmentation performance.

$$DSC = \frac{2 \times |P \cap G|}{|P| + |G|}, \quad (3)$$

where P represents the predicted segmentation. G represents the ground truth segmentation. $|P \cap G|$ represents the number of pixels in the intersection of the predicted and ground truth segmentations. $|P|$ represents the number of pixels in the predicted segmentation. $|G|$ represents the number of pixels in the ground truth segmentation.

Mean Intersection over Union (mIoU): mIoU calculates the average ratio of intersection over the union between the predicted segmentation and the ground truth across all classes. The mIoU ranges from 0 to 1, with higher values indicating better segmentation performance.

$$mIoU = \frac{1}{C} \sum_{i=1}^C \frac{|P_i \cap G_i|}{|P_i| + |G_i| - |P_i \cap G_i|}, \quad (4)$$

where C represents the number of classes. P_i represents the predicted segmentation for class i . G_i represents the ground truth segmentation for class i .

C. Comparisons with State-of-the-Art Methods

This subsection provides a detailed analysis of SMAFormer’s performance compared to state-of-the-art methods on three medical image segmentation datasets: LiTS2017, ISIDM2019, and Synapse. The results are summarized in Table I and II.

1) Liver Tumor Segmentation: The results are presented in Table I. SMAFormer demonstrates superior performance, achieving an average DSC of 94.11% and a mean IoU of 91.94%. This surpasses the performance of all other methods compared, including TransUNet (DSC: 93.28%, mIoU: 90.81%). This substantial improvement highlights SMAFormer’s effectiveness in segmenting small and irregularly shaped tumors. This can be attributed to the synergistic multi-attention mechanism’s ability to capture both local and global features, as well as the feature fusion modulator’s role in preserving crucial information across different scales.

2) Bladder Tumor Segmentation: The results can be found in Table I. SMAFormer again exhibits superior performance on this dataset, achieving an average DSC of 96.07% and a mean IoU of 94.67%. Although it only achieved limited improvement in terms of average value of bladder segmentation results, it improved the Dice coefficient by 2.18% on average in the experimental results of tumor segmentation compared to the second best model. The significant margin of improvement over existing methods showcases SMAFormer’s capability to accurately delineate bladder tumor boundaries, even in challenging medical images. This can be attributed to the enhanced multi-layer perceptron (E-MLP) within the SMA Transformer block, which effectively captures local contextual information crucial for precise segmentation. SMAFormer’s performance on this dataset further demonstrates its robustness and generalizability across different medical image modalities.

3) Multi-Organ Segmentation: The results can be found in Table II. As the task difficulty increases, SMAFormer’s performance slightly lags behind the comparison model in a few metrics. However, considering the overall average across multiple experiments, SMAFormer still achieves state-of-the-art results on the Synapse multi-organ segmentation dataset. Moreover, The best results were notably achieved by SMAFormer on some smaller organs. Additionally, it is worth mentioning that the Modulator retains some biases and weights from previous liver experiments, resulting in significantly better liver indices compared to other models. SMAFormer outperforms all other methods in terms of average DSC (86.08%) and

TABLE II
COMPARISON WITH STATE-OF-THE-ART MODELS ON THE SYNAPSE MULTI-ORGAN DATASET. THE BEST RESULTS ARE BOLDED WHILE THE SECOND BEST ARE UNDERLINED.

| Model | Average DSC(%) \uparrow | Aorta DSC(%) \uparrow | Gallbladder DSC(%) \uparrow | Kidney(Left) DSC(%) \uparrow | Kidney(Right) DSC(%) \uparrow | Liver DSC(%) \uparrow | Pancreas DSC(%) \uparrow | Spleen DSC(%) \uparrow | Stomach DSC(%) \uparrow |
|------------------------|------------------------------|----------------------------|----------------------------------|-----------------------------------|------------------------------------|----------------------------|-------------------------------|-----------------------------|------------------------------|
| ViT [23]+CUP [5] | 67.86 | 70.19 | 45.10 | 74.70 | 67.40 | 91.32 | 42.00 | 81.75 | 70.44 |
| R50-ViT [23]+CUP [5] | 71.29 | 73.73 | 55.13 | 75.80 | 72.20 | 91.51 | 45.99 | 81.99 | 73.95 |
| TransUNet [5] | 84.36 | 90.68 | <u>71.99</u> | 86.04 | 83.71 | 95.54 | 73.96 | 88.80 | 84.20 |
| SwinUNet [3] | 79.13 | 85.47 | 66.53 | 83.28 | 79.61 | 94.29 | 56.58 | <u>90.66</u> | 76.60 |
| UNETR [38] | 79.56 | 89.99 | 60.56 | 85.66 | 84.80 | 94.46 | 59.25 | 87.81 | 73.99 |
| Swin UNETR [7] | 73.51 | 82.94 | 60.96 | 80.41 | 71.14 | 91.55 | 56.71 | 77.46 | 66.94 |
| CoTr [45] | <u>85.72</u> | 92.96 | 71.09 | 85.70 | 85.71 | <u>96.88</u> | 81.28 | 90.44 | 81.74 |
| nnFormer [6] | 85.32 | 90.72 | 71.67 | 85.60 | <u>87.02</u> | 96.28 | 82.28 | 87.30 | 81.69 |
| SMAFormer(Ours) | 86.08 | <u>92.13</u> | 72.03 | 86.97 | 88.60 | 97.71 | <u>81.93</u> | 91.77 | <u>84.15</u> |

achieves the highest DSC scores for five out of the eight organs. SMAFormer’s strong performance on this challenging dataset underscores its potential for broader applicability in various multi-organ segmentation tasks. This consistent performance across multiple organs highlights the effectiveness of SMAFormer’s U-shaped architecture and skip connections in preserving both high-level semantic information and low-level spatial details. In summary, SMAFormer consistently outperforms existing state-of-the-art methods across diverse medical image segmentation tasks. Its superior performance can be attributed to the synergistic combination of its novel components: the SMA Transformer block, the feature fusion modulator, and the enhanced multi-layer perceptron. These results demonstrate SMAFormer’s potential as a powerful and versatile tool for advancing the field of medical image segmentation.

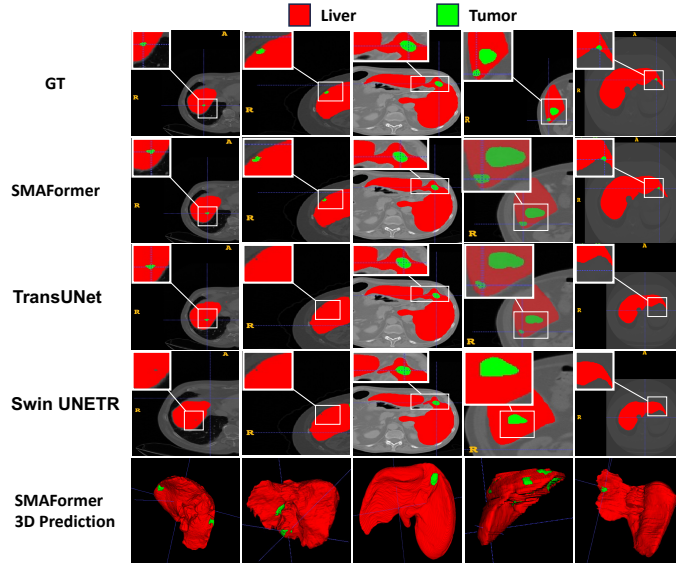


Fig. 3. LiTS2017 Prediction Result.

D. Visualization of Segmentation Results

To provide a qualitative assessment of SMAFormer’s segmentation capabilities, we present visual comparisons against

other state-of-the-art methods on all three datasets. Figure 3 showcases segmentation results on representative slices from the LiTS2017 dataset. SMAFormer demonstrates superior performance in segmenting both the liver and tumor boundaries compared to other methods. A close examination of the enlarged image in the upper left corner of each case reveals that the green color representing the tumor in the comparison model result figure disappears when the tumor is very small or there are multiple tumors. This occurs because even some advanced models may lose information after multiple layers of convolution. In contrast, SMAFormer accurately retains this crucial information after multiple layers of network training. SMAFormer accurately segments small tumor nodules in the liver periphery, which other methods struggle with.

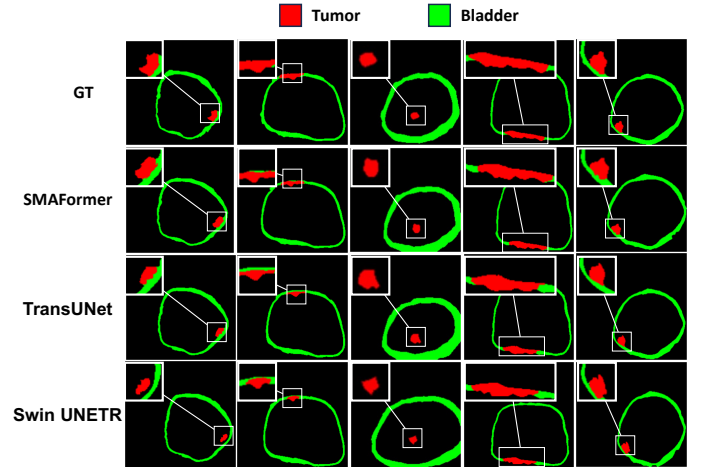


Fig. 4. ISICDM2019 Prediction Result.

Figure 4 illustrates segmentation outputs on challenging cases from the ISICDM2019 dataset. Although small tumors have irregular shapes and indistinct boundaries, the segmentation results from SMAFormer are noticeably closer to the ground truth compared to other methods.

Figure 5 presents segmentation results on the Synapse dataset, focusing on different abdominal organs. SMAFormer consistently produces accurate segmentations across various organs, demonstrating its robustness and generalization ability.

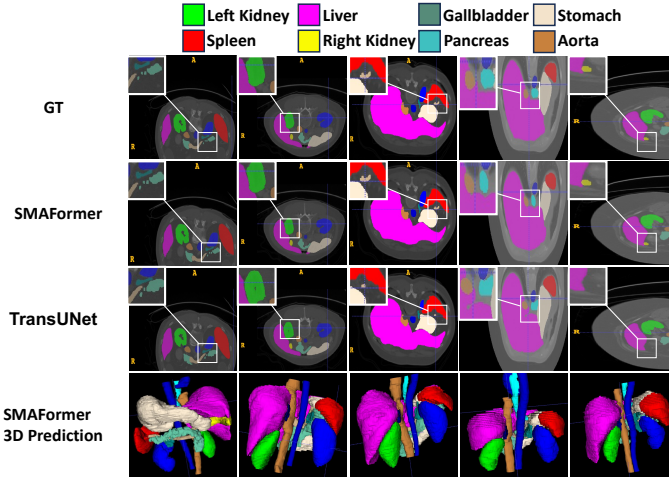


Fig. 5. Synapse Prediction Result.

SMAFormer accurately delineates the pancreas, a notoriously challenging organ to segment due to its variable shape and proximity to other organs.

E. Ablation Study

This subsection presents an ablation study to assess the impact of each component within SMAFormer. We conducted experiments on the ISICDM2019 and LiTS2017 datasets, using the same experimental setup as described in Section IV-A. Table III presents the results, highlighting the contribution of each component to the overall performance.

TABLE III
ABLATION STUDY OF DIFFERENT MODULES IN SMAFORMER.

| SMA | E-MLP | Modulator | ISICDM2019 Average DSC \uparrow | LiTS2017 Average DSC \uparrow |
|-----|-------|-----------|--------------------------------------|------------------------------------|
| ✓ | ✗ | ✗ | 82.28% | 79.95% |
| ✗ | ✓ | ✗ | 80.54% | 75.67% |
| ✗ | ✗ | ✓ | 78.41% | 73.20% |
| ✓ | ✓ | ✗ | 89.53% | 88.47% |
| ✓ | ✗ | ✓ | 86.31% | 84.26% |
| ✓ | ✓ | ✓ | 96.07% | 94.61% |

Effectiveness of SMA: To evaluate the effectiveness of the proposed SMA block, we replaced it with a standard Transformer block equipped with only multi-head self-attention. As evident from Table III this modification resulted in a performance drop across both datasets. This decline signifies the importance of integrating channel, spatial, and pixel attention for capturing comprehensive feature representations in medical images. The synergistic interplay of these attention mechanisms within the SMA block allows for a more nuanced understanding of the input data, leading to improved segmentation accuracy.

Impact of E-MLP: We investigated the contribution of the E-MLP module. We replaced the E-MLP with a standard FFN commonly used in Transformer architectures. This substitution led to a decrease in performance, as shown in Table III.

This outcome underscores the value of incorporating depth-wise and pixel-wise convolutions within the E-MLP. These convolutions enhance the model’s ability to capture local context, crucial for accurately delineating the boundaries of small structures like tumors.

Contribution of Multi-Scale Segmentation Modulator:

We examined the role of the multi-scale segmentation modulator. Removing this modulator from the SMAFormer architecture resulted in a noticeable performance degradation. This observation confirms the modulator’s significance in facilitating synergistic multi-attention and enhancing the network’s ability to capture fine-grained details. By embedding positional information, providing a trainable bias term, and streamlining multi-attention computations, the modulator contributes significantly to the overall efficacy of the SMAFormer model.

In summary, the ablation study demonstrates that each component of SMAFormer contributes to its superior performance in medical image segmentation. The synergistic multi-attention block, enhanced multi-layer perceptron, and multi-scale segmentation modulator work in concert to enable accurate and efficient segmentation of challenging medical images.

V. CONCLUSION

In this paper, we presented SMAFormer, a novel Transformer-based architecture designed for efficient and accurate medical image segmentation. The key innovation lies in the Synergistic Multi-Attention (SMA) block, which effectively integrates pixel, channel, and spatial attention mechanisms to capture both local and global contextual information. This synergistic approach addresses the limitations of conventional Transformers in accurately segmenting small and irregularly shaped tumors and organs commonly found in medical images. Furthermore, the introduction of a multi-scale segmentation modulator enhances SMAFormer’s ability to preserve salient features across different scales and further facilitates the synergistic interplay between the multiple attention mechanisms. Extensive experiments conducted on three publicly available medical image segmentation datasets demonstrate that SMAFormer achieves state-of-the-art performance, surpassing existing methods in accurately segmenting various organs and tumors. The promising results obtained in this study highlight the potential of SMAFormer as a robust and effective tool for assisting medical professionals in diagnosis, treatment planning, and disease monitoring. Future research will focus on exploring the application of SMAFormer to other medical imaging modalities and investigating its performance in more challenging clinical settings.

VI. ACKNOWLEDGMENT

This work was supported in part by the National Key R&D Project of China (2018YFA0704102, 2018YFA0704104), in part by Natural Science Foundation of Guangdong Province (No. 2023A1515010673), and in part by Shenzhen Technology Innovation Commission (No. JSGG20220831110400001), in part by Shenzhen Development and Reform Commission (No. XMHT20220104009), in part by the Science and

REFERENCES

- [1] G. P. Dunn, A. T. Bruce, H. Ikeda, L. J. Old, and R. D. Schreiber, "Cancer immunoediting: from immunosurveillance to tumor escape," *Nature immunology*, vol. 3, no. 11, pp. 991–998, 2002. [1](#)
- [2] A. Lin, B. Chen, J. Xu, Z. Zhang, G. Lu, and D. Zhang, "Ds-transunet: Dual swin transformer u-net for medical image segmentation," *IEEE Transactions on Instrumentation and Measurement*, vol. 71, pp. 1–15, 2022. [1](#)
- [3] H. Cao, Y. Wang, J. Chen, D. Jiang, X. Zhang, Q. Tian, and M. Wang, "Swin-unet: Unet-like pure transformer for medical image segmentation," in *ECCV*, 2022, pp. 205–218. [1](#), [5](#), [6](#)
- [4] B. Chen, Y. Liu, Z. Zhang, G. Lu, and A. W. K. Kong, "Transattunet: Multi-level attention-guided u-net with transformer for medical image segmentation," *IEEE Transactions on Emerging Topics in Computational Intelligence*, 2023. [1](#), [2](#)
- [5] J. Chen, Y. Lu, Q. Yu, X. Luo, E. Adeli, Y. Wang, L. Lu, A. L. Yuille, and Y. Zhou, "Transunet: Transformers make strong encoders for medical image segmentation," *ArXiv preprint*, vol. abs/2102.04306, 2021. [1](#), [2](#), [5](#), [6](#)
- [6] H.-Y. Zhou, J. Guo, Y. Zhang, X. Han, L. Yu, L. Wang, and Y. Yu, "nn-former: volumetric medical image segmentation via a 3d transformer," *IEEE Transactions on Image Processing*, 2023. [1](#), [4](#), [5](#), [6](#)
- [7] Y. Tang, D. Yang, W. Li, H. R. Roth, B. Landman, D. Xu, V. Nath, and A. Hatamizadeh, "Self-supervised pre-training of swin transformers for 3d medical image analysis," in *CVPR*, 2022, pp. 20 730–20 740. [1](#), [5](#), [6](#)
- [8] G. Xu, X. Zhang, X. He, and X. Wu, "Levit-unet: Make faster encoders with transformer for medical image segmentation," in *PRCV*, 2023, pp. 42–53. [1](#)
- [9] G. Li, X. He, W. Zhang, H. Chang, L. Dong, and L. Lin, "Non-locally enhanced encoder-decoder network for single image de-raining," in *ACM MM*, 2018, pp. 1056–1064. [1](#)
- [10] J. Ruan, S. Xiang, M. Xie, T. Liu, and Y. Fu, "Malunet: A multi-attention and light-weight unet for skin lesion segmentation," in *BIBM*. IEEE, 2022, pp. 1150–1156. [1](#)
- [11] F. I. Diakogiannis, F. Waldner, P. Caccetta, and C. Wu, "Resunet-a: A deep learning framework for semantic segmentation of remotely sensed data," *ISPRS Journal of Photogrammetry and Remote Sensing*, vol. 162, pp. 94–114, 2020. [1](#), [2](#)
- [12] Y. Li, K. Zhang, J. Cao, R. Timofte, and L. Van Gool, "Localvit: Bringing locality to vision transformers," *arXiv preprint arXiv:2104.05707*, 2021. [1](#)
- [13] K. Yuan, S. Guo, Z. Liu, A. Zhou, F. Yu, and W. Wu, "Incorporating convolution designs into visual transformers," in *WACV*, 2021, pp. 579–588. [1](#)
- [14] S. W. Zamir, A. Arora, S. Khan, M. Hayat, F. S. Khan, M.-H. Yang, and L. Shao, "Multi-stage progressive image restoration," in *CVPR*, 2021, pp. 14 821–14 831. [1](#)
- [15] H. Zhang, Y. Dai, H. Li, and P. Koniusz, "Deep stacked hierarchical multi-patch network for image deblurring," in *CVPR*, 2019, pp. 5978–5986. [1](#)
- [16] O. Kupyn, V. Budzan, M. Mykhailych, D. Mishkin, and J. Matas, "Deblurgan: Blind motion deblurring using conditional adversarial networks," in *CVPR*, 2018, pp. 8183–8192. [1](#)
- [17] O. Kupyn, T. Martyniuk, J. Wu, and Z. Wang, "Deblurgan-v2: Deblurring (orders-of-magnitude) faster and better," in *ICCV*, 2019, pp. 8878–8887. [1](#)
- [18] O. Ronneberger, P. Fischer, and T. Brox, "U-net: Convolutional networks for biomedical image segmentation," in *MICCAI*, 2015, pp. 234–241. [2](#)
- [19] K. He, X. Zhang, S. Ren, and J. Sun, "Deep residual learning for image recognition," in *CVPR*, 2016, pp. 770–778. [2](#)
- [20] C. Szegedy, S. Ioffe, V. Vanhoucke, and A. A. Alemi, "Inception-v4, inception-resnet and the impact of residual connections on learning," in *AAAI*, 2017, pp. 4278–4284. [2](#)
- [21] K. Zhang, W. Zuo, Y. Chen, D. Meng, and L. Zhang, "Beyond a gaussian denoiser: Residual learning of deep cnn for image denoising," *IEEE transactions on image processing*, vol. 26, no. 7, pp. 3142–3155, 2017. [2](#)
- [22] Z. Zhou, M. M. R. Siddiquee, N. Tajbakhsh, and J. Liang, "Unet++: Redesigning skip connections to exploit multiscale features in image segmentation," *IEEE Transactions on Medical Imaging*, 2019. [2](#)
- [23] A. Dosovitskiy, L. Beyer, A. Kolesnikov, D. Weissenborn, X. Zhai, T. Unterthiner, M. Dehghani, M. Minderer, G. Heigold, S. Gelly, J. Uszkoreit, and N. Houlsby, "An image is worth 16x16 words: Transformers for image recognition at scale," in *ICLR*, 2021. [2](#), [5](#), [6](#)
- [24] Z. Liu, Y. Lin, Y. Cao, H. Hu, Y. Wei, Z. Zhang, S. Lin, and B. Guo, "Swin transformer: Hierarchical vision transformer using shifted windows," in *ICCV*, 2021, pp. 9992–10 002. [2](#)
- [25] Q. Zhang and Y. Yang, "Rest: An efficient transformer for visual recognition," in *NeurIPS*, 2021, pp. 15 475–15 485. [2](#)
- [26] Q. Zhang and Y.-B. Yang, "Rest v2: simpler, faster and stronger," *NeurIPS*, vol. 35, pp. 36 440–36 452, 2022. [2](#), [5](#)
- [27] O. Oktay, J. Schlemper, L. L. Folgoc, M. Lee, M. Heinrich, K. Misawa, K. Mori, S. McDonagh, N. Y. Hammerla, B. Kainz *et al.*, "Attention u-net: Learning where to look for the pancreas," *ArXiv preprint*, vol. abs/1804.03999, 2018. [2](#)
- [28] Y. Chang, H. Menghan, Z. Guangtao, and Z. Xiao-Ping, "Transclaw u-net: Claw u-net with transformers for medical image segmentation," *ArXiv preprint*, vol. abs/2107.05188, 2021. [2](#)
- [29] D. Jha, P. H. Smedsrud, D. Johansen, T. de Lange, H. D. Johansen, P. Halvorsen, and M. A. Riegler, "A comprehensive study on colorectal polyp segmentation with resunet++, conditional random field and test-time augmentation," *IEEE journal of biomedical and health informatics*, vol. 25, no. 6, pp. 2029–2040, 2021. [2](#), [5](#)
- [30] Z. Wang, X. Cun, J. Bao, W. Zhou, J. Liu, and H. Li, "Uformer: A general u-shaped transformer for image restoration," in *CVPR*, 2022, pp. 17 683–17 693. [2](#), [3](#)
- [31] H. Wu, B. Xiao, N. Codella, M. Liu, X. Dai, L. Yuan, and L. Zhang, "Cvt: Introducing convolutions to vision transformers," in *ICCV*, 2021, pp. 22–31. [3](#)
- [32] T. Huang, S. Li, X. Jia, H. Lu, and J. Liu, "Neighbor2neighbor: Self-supervised denoising from single noisy images," in *CVPR*, 2021, pp. 14 781–14 790. [3](#)
- [33] Y. Li, K. Zhang, J. Cao, R. Timofte, and L. Van Gool, "Localvit: Bringing locality to vision transformers," *arXiv preprint arXiv:2104.05707*, 2021. [3](#)
- [34] M. Sandler, A. Howard, M. Zhu, A. Zhmoginov, and L.-C. Chen, "Mobilenetv2: Inverted residuals and linear bottlenecks," in *CVPR*, 2018, pp. 4510–4520. [3](#)
- [35] K. Yuan, S. Guo, Z. Liu, A. Zhou, F. Yu, and W. Wu, "Incorporating convolution designs into visual transformers," in *ICCV*, 2021, pp. 579–588. [3](#)
- [36] D. Hendrycks and K. Gimpel, "Gaussian error linear units (gelus)," *arXiv preprint arXiv:1606.08415*, 2016. [3](#)
- [37] F. Milletari, N. Navab, and S.-A. Ahmadi, "V-net: Fully convolutional neural networks for volumetric medical image segmentation," in *3DV*, 2016, pp. 565–571. [4](#)
- [38] A. Hatamizadeh, Y. Tang, V. Nath, D. Yang, A. Myronenko, B. Landman, H. R. Roth, and D. Xu, "Unetr: Transformers for 3d medical image segmentation," in *WACV*, 2022, pp. 574–584. [5](#), [6](#)
- [39] P. B. *et al.*, "The liver tumor segmentation benchmark (lits)," *ArXiv preprint*, vol. abs/1901.04056, 2019. [4](#)
- [40] *Proceedings of the Third International Symposium on Image Computing and Digital Medicine, ISICDM 2019, Xi'an, China, August 24-26, 2019*, 2019. [4](#)
- [41] B. Landman, Z. Xu, J. Igelsias, M. Styner, T. Langerak, and A. Klein, "Miccai multi-atlas labeling beyond the cranial vault-workshop and challenge," in *MICCAI*, vol. 5, 2015, p. 12. [4](#)
- [42] J. Duchi, E. Hazan, and Y. Singer, "Adaptive subgradient methods for online learning and stochastic optimization," *Journal of machine learning research*, vol. 12, no. 7, 2011. [4](#)
- [43] A. Dosovitskiy, L. Beyer, A. Kolesnikov, D. Weissenborn, X. Zhai, T. Unterthiner, M. Dehghani, M. Minderer, G. Heigold, S. Gelly *et al.*, "An image is worth 16x16 words: Transformers for image recognition at scale," *arXiv preprint arXiv:2010.11929*, 2020. [5](#)
- [44] J. Chen, J. Mei, X. Li, Y. Lu, Q. Yu, Q. Wei, X. Luo, Y. Xie, E. Adeli, Y. Wang *et al.*, "3d transunet: Advancing medical image segmentation through vision transformers," *arXiv preprint arXiv:2310.07781*, 2023. [5](#)
- [45] Y. Xie, J. Zhang, C. Shen, and Y. Xia, "Cotr: Efficiently bridging cnn and transformer for 3d medical image segmentation," in *MICCAI*, 2021, pp. 171–180. [6](#)
- [46] L. R. Dice, "Measures of the amount of ecologic association between species," *Ecology*, vol. 26, no. 3, pp. 297–302, 1945. [5](#)